Pis'ma v ZhETF, vol. 101, iss. 12, pp. 897 – 901 © 2015 June 25

The ferromagnetic origin of Mn-doped $Sr_3La_2O_5Zn_2As_2$: a first-principles study

L. Hua[1)], *Q. L. Zhu*

Nanjing Normal University Taizhou College, 225300 Taizhou, China

Submitted 6 May 2015

We have investigated the electronic structure and magnetic properties of Mn-doped $Sr_3La_2O_5Zn_2As_2$ using density functional theory within the generalized gradient approximation (GGA)+U schemes. We have shown that the ground state magnetic structure of Mn-doped $Sr_3La_2O_5Zn_2As_2$ is antiferromagnetic. Zn vacancies and hole-mediated Zener's $p-d$ exchange are responsible for the origin of ferromagnetism.

DOI: 10.7868/S0370274X1512005X

1. Introduction. The dilute magnetic semiconductors (DMS) are nonmagnetic semiconductors doped with magnetic elements, which display ferromagnetic ordering below the Curie temperature (T_c). Mn-doped GaAs is the most investigated DMS and its magnetic properties are well established experimentally [1–3]. In (Ga,Mn)As the Mn substituting for the trivalent Ga cation acts as both an acceptor and a spin source of magnetic moments simultaneously. Moreover, during the fabrication of (Ga,Mn)As thin films, some Mn atoms enter interstitial sites and behave as a double donor, which make it difficult to determine precisely the amount of Mn substituting Ga at ionic sites. Seeking for the new ferromagnetic semiconductor systems with more controllable charge and spin densities might be helpful to understand the general mechanism of ferromagnetism in DMS.

A new type of ferromagnetic DMS that overcomes these difficulties has been discovered recently. Bulk specimens of Li(Zn,Mn)As were successfully fabricated, using excess Li concentrations introduced into hole carriers, while independently making the isovalent substitution of Mn^{2+} for Zn^{2+} to achieve local spin doping [4]. Shortly after, Li(Zn,Mn)P with $T_c \sim 40$ K were also fabricated by doping Mn into the I–II–V direct gap semiconductors LiZnP [5]. LiZnPn (Pn = P, As) can be viewed as a derivative of the third family of Fe-based superconductors LiFeAs. Accordingly, the first family of Fe-based superconductor is 1111-type oxypnictides $LaFeAs(O_{1-x}F_x)$. With identical Two-dimensional crystal structure, three 1111 type DMS systems, (La,Ba)(Zn,Mn)AsO with $T_c \sim 40$ K [6], (La,Ca)(Zn,Mn)SbO with $T_c \sim 40$ K [7], (La,Sr)(Cu,Mn)SO with $T_c \sim 210$ K [8] have been reported. Similarly, two bulk form DMS systems, $(Ba,K)(Zn,Mn)_2As_2$ [9] with $T_c \sim 180$ K and $(Ba,K)(Cd,Mn)_2As_2$ [10] with $T_c \sim 17$ K, have been reported. These two systems are structurally identical to that of 122 type iron pnictides superconductor $(Ba,K)Fe_2As_2$. The fourth family of Fe-based superconductors is 11 type $FeSe_{1+\delta}$, which can be paralleled to the well investigated II-VI DMS, i.e., (Zn,Mn)Se. There are two more families of Fe-based superconductors, namely, 32522 type $(Ca_3Al_2O_5)Fe_2As_2$ and 42622 type $Sr_4V_2O_6Fe_2As_2$. Very recently, 32522 type DMS $Sr_3La_2O_5(Zn,Mn)_2As_2$ with $T_c \sim 40$ K has been reported [11]. In this paper, we have performed a first-principles density functional theory study on $Sr_3La_2O_5(Zn,Mn)_2As_2$ and discussed its ferromagnetic origin.

2. Computational method. The first-principles calculations were performed by using density functional theory (DFT) method within the Perdew–Burke–Ernzerhof (PBE) generalized gradient approximation (GGA) [12], implemented in the Vienna *ab initio* Simulation Package (VASP) [13]. The strong-correlated correction was considered with GGA+U method [14] to deal with the Mn's $3d$ electrons. The effective onsite Coulomb interaction parameter (U) and exchange interaction parameter (J) are set to be 4.0 and 1.0 eV for Mn's $3d$ electrons. These values have been tested and used in the previous experimental and theoretical works [15–17]. For Zn atoms, the strong-correlated correction was not applied as their $3d$ orbitals are fully occupied. $4s4p5s$ for Sr, $5p5d6s$ for La, $2s2p$ for O, $3d4s$ for Zn, $3d4s$ for Mn, and $4s4p$ for As were treated as valence orbitals in the calculations. The projector augmented wave (PAW) potential [18] and the plane waves cut-off energy of 300 eV were used. For $Sr_3La_2O_5Zn_2As_2$ unit cell, a Γ-centered Monkhorst–Pack [19] k-point mesh of

[1)]e-mail: pjsd@163.com

$5\times5\times1$ was used and the internal atomic coordinates were relaxed until the force was less than 0.01 eV/Å. For Mn-doped $Sr_3La_2O_5Zn_2As_2$ supercell, a Γ-centered Monkhorst–Pack k-point mesh of $3\times3\times1$ was used. The criterion for the total energy was set as 10^{-4} eV.

3. Results and discussion. As a parent system, $Sr_3La_2O_5Zn_2As_2$ crystallizes in the tetragonal $Ca_3Al_2O_5Fe_2As_2$-type crystal structure with the space group $I4/mmm$, as shown in Fig. 1. The experimentally measured lattice constant of $Sr_3La_2O_5Zn_2As_2$ ($a = 4.2612$ Å, $c = 27.675$ Å) was used in our calculations [11] and the internal coordinates were optimized. We have used two Mn atoms to substitute two Zn atoms in a $2\times2\times1$ supercell for constructing $Sr_3La_2O_5(Zn_{0.875}Mn_{0.125})_2As_2$, as shown in Fig. 2. We have calculated the first nearest neighboring (indicating Mn1–Mn2) and the second nearest neighboring (indicating Mn1–Mn3) pair configuration. Table 1 lists the energy of the $Sr_3La_2O_5(Zn_{0.875}Mn_{0.125})_2As_2$ with ferromagnetic (FM) and antiferromagnetic (AFM) state for the first nearest neighboring and the second nearest neighboring configuration.

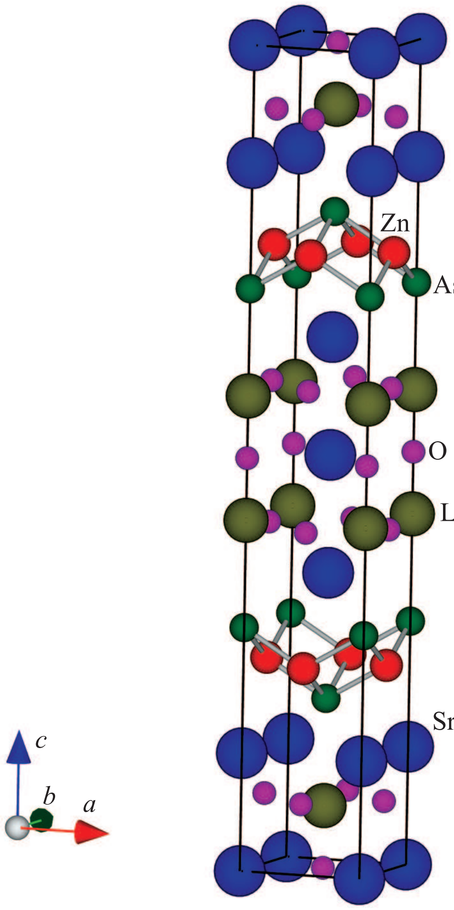

Fig. 1. The crystal structure of the $Sr_3La_2O_5Zn_2As_2$ unit cell. Blue, dark yellow, magenta, red and olive spheres represent Sr, La, O, Zn, and As atoms, respectively

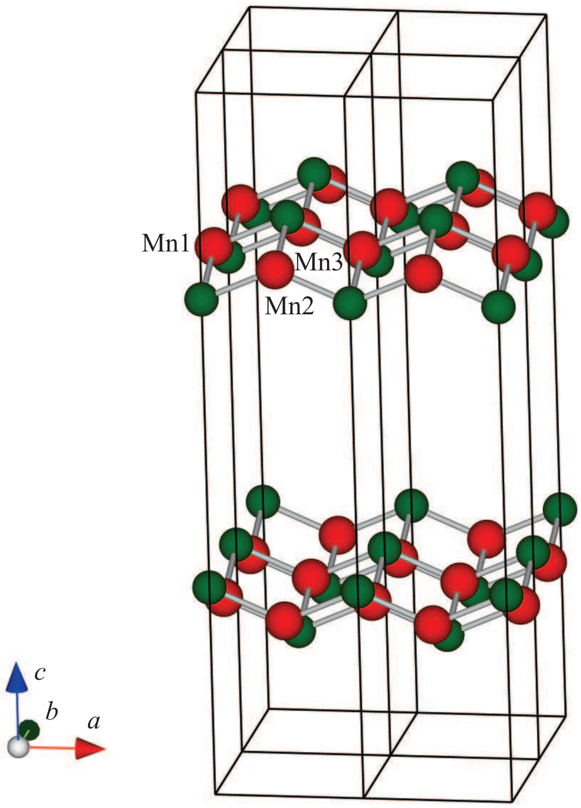

Fig. 2. The $2\times2\times1$ supercell of $Sr_3La_2O_5(Zn_{0.875}Mn_{0.125})_2As_2$. The configurations of Mn–Mn pair indicate Mn1–Mn2 and Mn1–Mn3. For seeing clearly, we omit the Sr, La, and O atoms

Table 1

The total energy (eV) of different configuration of ferromagnetic and antiferromagnetic state of $Sr_3La_2O_5(Zn_{0.875}Mn_{0.125})_2As_2$

Configuration	E_{FM}	E_{AFM}	$E_{AFM}-E_{FM}$
Mn1–Mn2	−640.1453	−640.3147	−0.1694
Mn1–Mn3	−640.2163	−640.3094	−0.0931

Our calculations show that the energy of AFM state is lower than FM for Mn1–Mn2 and Mn1–Mn3 configuration. This means that the ground state of $Sr_3La_2O_5(Zn_{0.875}Mn_{0.125})_2As_2$ should be AFM state. In Fig. 3, we show the spin-polarized DOS of $Sr_3La_2O_5(Zn_{0.875}Mn_{0.125})_2As_2$ of Mn1–Mn2 AFM configuration. We see that the contributions from the Mn $4s$ states to the valence bands of $Sr_3La_2O_5(Zn_{0.875}Mn_{0.125})_2As_2$ are negligible. So the

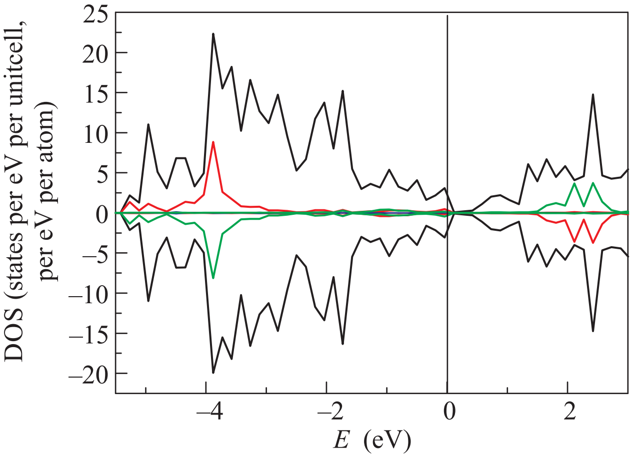

Fig. 3. The total averaged (black line) density of states of $Sr_3La_2O_5(Zn_{0.875}Mn_{0.125})_2As_2$ per unit cell. The partial density of states of Mn1 $3d$ (red line), $4s$ (blue line) and Mn2 $3d$ (green line), $4s$ (blue line) per atom. The energy zero is taken at the Fermi level and indicated by the vertical line

Mn atoms are in the form of cation Mn^{2+}. The Mn1 $3d$ major states are occupied and minor states empty while Mn2 $3d$ states are reverse. This means that the superexchange mechanism [20] leads to the antiferromagnetic coupling between the two Mn atoms. From Fig. 3, we also see that the exchange splitting, due to the Mn $3d$ electrons localizing and onsite coulomb interaction, is larger than the crystal filed splitting. This leads to a high spin configuration of d^5 with the local magnetic moments of Mn atoms with $S = 5/2$, which is consistent with our calculated moment $4.15\mu_B$. However, the experiments [11] show that $Sr_3La_2O_5(Zn_{1-x}Mn_x)_2As_2$ ($x = 0.05, 0.1, 0.2$) is FM state with $T_c \sim 40$ K. Taking into account the appearance of secondary phases of Zn_3As_2 and Sr_2As for $x \leq 0.1$, we speculate that the different magnetic property between experimental samples and our calculated pure Mn-doped $Sr_3La_2O_5Zn_2As_2$ may come from the intrinsic defects in the experimental samples. Because the carriers type is not accurately determined by experiments [11], we introduce electron and hole carriers doping into $Sr_3La_2O_5(Zn_{0.875}Mn_{0.125})_2As_2$, respectively. In Fig. 4, the total energy differences between AFM and FM states are plotted versus the concentration of doped carriers. The positive and negative values are for electron and hole doping, respectively. As shown in the Fig. 4, independent of the Mn–Mn configuration, the AFM state is stable with electron carriers. However, as for hole carriers, increasing the hole doping concentration induces a AFM–FM transition in the $Sr_3La_2O_5(Zn_{0.875}Mn_{0.125})_2As_2$ compound. We think that the hole carriers induce the FM state, which has been observed experimentally in the Mn-doped $Sr_3La_2O_5Zn_2As_2$. In order to see the origin of the carrier induced ferromagnetism. The total and partial density of states of Mn $3d$, As $4p$, and O $2p$ states are shown in Fig. 5. The DOS in Fig. 5 shows the semi-metallic behavior for the compound at the Fermi level. The hole carriers are introduced into the empty states near the Fermi level, which is mostly composed of the As $4p$ states. So the delocalized holes have a character of the host states near the top of the valence band with a small admixture of the Mn $3d$

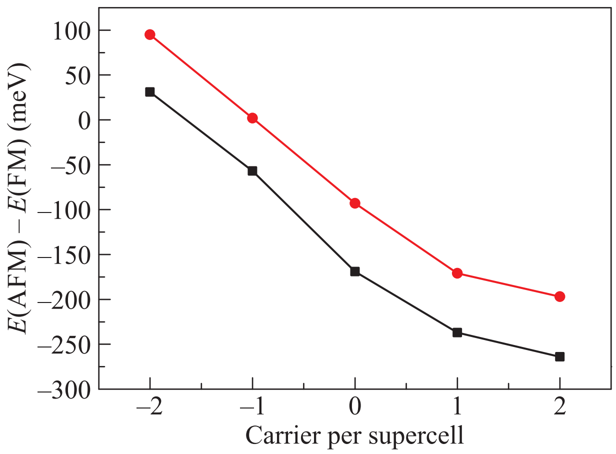

Fig. 4. The total energy difference between AFM and FM states with the concentration of doping carriers for the Mn1–Mn2 (black line) and Mn1–Mn3 (red line) configurations

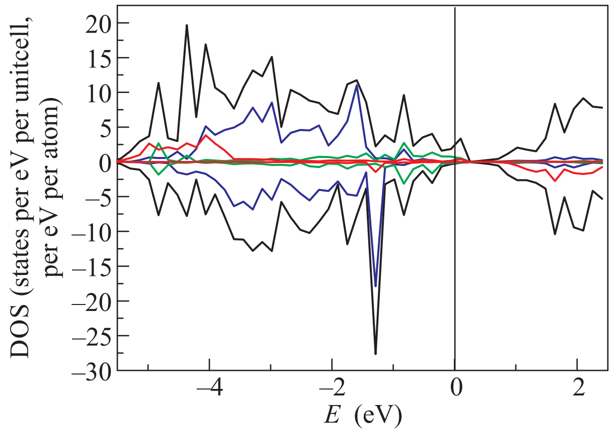

Fig. 5. The total averaged (black line) density of states of $Sr_3La_2O_5(Zn_{0.875}Mn_{0.125})_2As_2$ and the partial density of states of O $2p$ (blue line), As $4p$ (green line) with hole carriers per unit cell. The partial density of states of Mn $3d$ (red line) per atom. The energy zero is taken at the Fermi level and indicated by the vertical line

orbital weight. At the same time, the main peak in the partial density of states of the majority spin Mn $3d^5$ electrons is well below the Fermi level and these states form a local moment. Thus, the ferromagnetic coupling between Mn local moments is mediated by delocalized band holes via Zener's *p–d* exchange interaction [20].

To investigate the source of the hole carriers, we calculated the formation energy of different acceptor defect in the Mn-doped $Sr_3La_2O_5Zn_2As_2$. There are Sr vacancy (V_{Sr}), La vacancy (V_{La}), Zn vacancy (V_{Zn}), O interstitial (O_{int}), and As interstitial (As_{int}). The defect formation energy E_f is calculated from [21]

$$E_f = E_t - E_b \pm E_a,$$

where E_t is the total energy of the Mn-doped $Sr_3La_2O_5Zn_2As_2$ supercell with an acceptor defect; E_b is the corresponding energy of the bulk Mn-doped $Sr_3La_2O_5Zn_2As_2$ supercell; E_a is the energy of an isolated atom. Vacancy defect used "+" while interstitial defect "−". Table 2 lists the formation energy E_f of different defect. The Zn vacancy have the lowest formation energy among these defects and is the most stable defect in Mn-doped $Sr_3La_2O_5Zn_2As_2$. So the source of the hole carriers is Zn vacancy.

Table 2

The calculated formation energy E_f of different Mn–Mn configuration

Configuration	Defect	E_f
Mn1–Mn2	V_{Sr}	3.31
	V_{La}	13.
	V_{Zn}	2.71
	O_{int}	7.65
	As_{int}	25.42
Mn1–Mn3	V_{Sr}	3.24
	V_{La}	13.04
	V_{Zn}	2.73
	O_{int}	7.59
	As_{int}	25.76

4. Summary. In conclusion, we have performed a study of the electronic structure and magnetic properties of Mn-doped $Sr_3La_2O_5Zn_2As_2$ using density functional theory within the GGA+U schemes. We have shown that the superexchange mechanism leads to the antiferromagnetic coupling between Mn atoms in Mn-doped $Sr_3La_2O_5Zn_2As_2$. The ferromagnetic origin of experimental Mn-doped $Sr_3La_2O_5Zn_2As_2$ is hole carriers mediated via Zener's *p–d* exchange interaction. Zn vacancy is the origin of hole carriers.

1. H. Ohno, A. Shen, F. Matsukura, A. Oiwa, A. Endo, S. Katsumoto, and Y. Iye, Appl. Phys. Lett. **69**, 363 (1996).
2. T. Jungwirth, J. Sinova, J. Mašek, J. Kučera, and A. H. MacDonald, Rev. Mod. Phys. **78**, 809 (2006).
3. T. Dietl and H. Ohno, Rev. Mod. Phys. **86**, 187 (2014).
4. Z. Deng, C. Q. Jin, Q. Q. Liu, X. C. Wang, J. L. Zhu, S. M. Feng, L. C. Chen, R. C. Yu, C. Arguello, T. Goko, F. Ning, J. Zhang, Y. Wang, A. Aczel, T. Munsie, T. J. Williams, G. M. Luke, T. Kakeshita, S. Uchida, W. Higemoto, T. U. Ito, B. Gu, S. Maekawa, G. D. Morris, and Y. J. Uemura, Nat. Comm. **2**, 041102R (2013).
5. Z. Deng, K. Zhao, B. Gu, W. Han, J. L. Zhu, X. C. Wang, X. Li, Q. Q. Liu, R. C. Yu, T. Goko, B. Frandsen, L. Liu, J. S. Zhang, Y. Y. Wang, F. L. Ning, S. Maekawa, Y. J. Uemura, and C. Q. Jin, Phys. Rev. B **88**, 081203(R) (2013).
6. C. Ding, H. Man, C. Qin, J. Lu, Y. Sun, Q. Wang, B. Yu, C. Feng, T. Goko, C. J. Arguello, L. Liu, B. A. Frandsen, Y. J. Uemura, H. Wang, H. Luetkens, E. Morenzoni, W. Han, C. Q. Jin, T. Munsie, T. J. Williams, R. M. D'Ortenzio, T. Medina, G. M. Luke, T. Imai, and F. L. Ning, Phys. Rev. B **88**, 041102R (2013).
7. W. Han, K. Zhao, X. C. Wang, Q. Q. Liu, F. L. Ning, Z. Deng, Y. Liu, C. Ding, and C. Q. Jin, Sci. China. Phys. Mech. Astron. **56**, 2026 (2013).
8. X. J. Yang, Y. K. Li, C. Y. Shen, B. Q. Si, Y. L. Sun, Q. Tao, C. Cao, Z. A. Xu, and F. C. Zhang, Appl. Phys. Lett. **103**, 022410 (2013).
9. K. Zhao, Z. Deng, X. C. Wang, W. Han, J. L. Zhu, X. Li, Q. Q. Liu, T. Goko, B. Frandsen, L. Liu, F. L. Ning, Y. J. Uemura, H. Dabkovska, G. M. Luke, H. Leutkens, E. Molenzoni, S. R. Dunsiger, A. Senyshyn, P. Boeni, and C. Q. Jin, Nat. Comm. **4**, 1422 (2013).
10. X. J. Yang, Y. K. Li, P. Zhang, Y. K. Luo, Q. Chen, C. M. Feng, C. Cao, J. H. Dai, Q. Tao, G. H. Cao, and Z. A. Xu, J. Appl. Phys. **114**, 223905 (2013).
11. H. Y. Man, C. Qin, C. Ding, Q. Wang, X. Gong, S. L. Guo, H. D. Wang, B. Chen, and F. L. Ning, EPL **105**, 67004 (2014).
12. J. P. Perdew, K. Burke, and M. Ernzerhof, Phys. Rev. Lett. **77**, 3865 (1996).
13. G. Kresse and J. Furthmüller, Phys. Rev. B **54**, 11169 (1996).
14. A. I. Liechtenstein, V. I. Anisimov, and J. Zaanen, Phys. Rev. B **52**, R5467 (1995).
15. J. Okabayashi, A. Kimura, O. Rader, T. Mizokawa, A. Fujimori, T. Hayashi, and M. Tanaka, Phys. Rev. B **58**, 4211 (1998).
16. K. Sato, P. H. Dederichs, H. Katayama, and J. Kudrnovsky, J. Phys.: Cond. Mat. **16**, 5491 (2004).
17. M. Wierzbowska, D. Sanchez, and S. Sanvito, Phys. Rev. B. **70**, 235209 (2004).

18. P. E. Blöchl, Phys. Rev. B **50**, 17953 (1994).
19. H. J. Monkhorst and J. D. Pack, Phys. Rev. B **13**, 5188 (1976).
20. K. Sato, L. Bergqvist, J. Kudrnovsky, P. H. Dederichs, O. Eriksson, I. Turek, B. Sanyal, G. Bouzerar, H. Katayama-Yoshida, V. A. Dinh, T. Fukushima, H. Kizaki, and R. Zeller, Rev. Mod. Phys. **82**, 1633 (2010).
21. H. Pan, Y. P. Feng, Q. Y. Wu, Z. G. Huang, and J. Y. Lin, Phy. Rev. B **77**, 125211 (2008).